Forensics of polymer networks

Andrey Dobrynin, Yuan Tian, Michael Jacobs, Evgeniia Nikitina, Dimitri Ivanov, Mitchell Maw, Foad Vashahi, Sergei Sheiko

Forensics of Polymer Networks

Andrey V. Dobrynin*, Yuan Tian, Michael Jacobs, Evgeniia A. Nikitina,[2] Dimitri A. Ivanov,[2,3] Mitchell Maw, Foad Vashahi, Sergei S. Sheiko*

[1] *Department of Chemistry, University of North Carolina at Chapel Hill, North Carolina, 27599, United States*

[2] *Faculty of Chemistry, Lomonosov Moscow State University, Leninskie Gory 1/51, Moscow 119991, Russia*

[3] *Institut de Sciences des Matériaux de Mulhouse-IS2M, CNRS UMR 7361, 15, rue Jean Starcky, F-68057 Mulhouse, France*

Polymer networks play a significant role in our lives from rubber to biological tissues[1-6]. It is understood that their characteristic properties – elasticity, strain-stiffening, and stretchability – are controlled by a convolution of chemical composition, strand conformation, and network topology[1-6]. Yet, since the discovery of rubber vulcanization by Charles Goodyear in 1839, the internal organization of networks has remained a sealed "black box". While many studies show how network properties respond to variation of structural parameters, no method currently exists that would allow decoding the structure of an arbitrary network from its properties[7]. We address this problem by developing a forensic-style method based on the analysis of the non-linear response to deformation of polymer networks to quantify their crosslink density, strand flexibility, and fraction of stress-supporting strands. The decoded structural information enables quality control of network synthesis, comparison of targeted to actual architecture, and classification of network types according to the effectiveness of stress distribution. The developed forensic approach is a vital step in future implementation of artificial intelligence principles for soft matter design.

The topology of polymer networks is an ill-defined product of erratic node formation processes. Any reasonable efforts to project network architecture by specifying stoichiometry and the synthetic pathway are instantly scrambled by swift scaffold percolation generating a stochastic distribution of structural elements (Fig. 1a)[1-4]. The problem is further exacerbated by the inability of traditional characterization techniques to isolate and measure contributions from the individual structural elements presenting polymer networks as a sealed "black box" (Fig. 1b)[7]. There are two general approaches, both imperative, to uncover network organization. The so-called *structure-to-property* approach employs model networks with synthetically pre-defined strands, loops, and dangles to quantify the vital contributions of each element to a specific property, e.g. modulus.[8-10] Although informative, this method is unsuitable for conventional polymer networks with unknown topology. Alternatively, a *structure-from-property* approach allows extraction of structural information of an arbitrary network from its properties. Current examples include the use of elastic modulus or equilibrium swelling ratio for gaining insight on crosslink density[1,2], however, this single parameter analysis is not sufficient to deconvolute the contributions from multiple structural elements. Even the seemingly trivial crosslink density is actually unknown.

We address this problem by developing a general framework for deciphering the network structure from its non-linear response to deformation (Fig. 1c). Unlike the traditional analysis of a single data point, e.g., modulus at small deformations[1,2,4,10], we analyze the entire shape of a stress-strain curve, containing information about the network structure. By expanding the analysis to multiple self-similar networks, we use their cross-correlated mechanical response to quantify the strand Kuhn length, density of stress-supporting strands, onset of entanglement-defined elasticity, and, in some cases, effective crosslink functionality and loop contributions. Our

approach can be viewed as a macroscopic analog of single chain stretching experiments that utilize large deformations to extract molecular information[11,12].

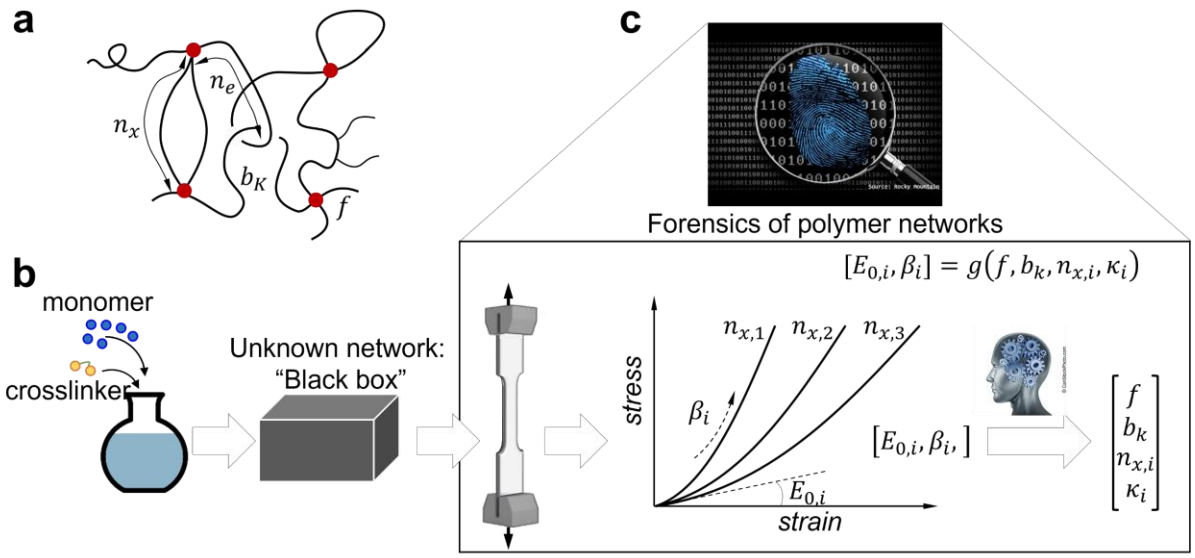

Figure 1. Forensics methodology. a, Schematics of a real polymer network (containing various defects such as loops, multiple strands, side chains, and dangles) defined by a set of structural parameters: degree of polymerization between crosslinks (red dots), n_x, and entanglements, n_e, crosslink functionality, f, and Kuhn length of network strand, b_K. **b,** An as-prepared network represents a black box with unknown internal organization - subjected to a forensic analysis. **c,** Workflow of our forensic procedure: (i) synthesis of a series of self-similar networks differing in crosslink density, (ii) deformation test to record non-linear stress-strain curves characterized by the Young's modulus, $E_{0,i}$, and strain-stiffening parameter, β_i, and (iii) deciphering network structure from the domain of the measured $[E_{0,i}, \beta_i]$ combinations to deliver the structural parameters $[f, b_K, n_x, \kappa]$, where κ is the network quality factor defined later.

The developed methodology does not require any assumptions about the type of structural defects[10,13], the mechanism of network assembly[10,14,15], nor solvent quality in swelling tests[1,2] to establish structure-property relationships. Unlike spectroscopic[16] and scattering[17] techniques that involve complex structure-perturbing preparation procedures, our method deals with as-synthesized materials intended for direct use in practical applications. Our approach takes into account contributions from crosslinks, defects (loops and dangling ends), and trapped entanglements (Fig.1a)[1,13,18] responsible for elastic modulus at small deformations, E_0, as well as

its strain-stiffening at large deformations due to finite strand extensibility, β. The only requirement is to have a series of networks with varying crosslink density prepared by the same synthesis protocol. Analysis of a single network is also possible but delivers less information.

The universality of the developed methodology was validated by applying the forensic approach to a broad set of elastomers including natural rubber[19], end-crosslinked linear poly(dimethyl siloxane) (PDMS)[9], and brush-like poly(n-butyl acrylate) (PBA) networks with systematically varied $n_{sc} = 0 - 41$, $n_{\mathrm{g}} = 1 - 10$, and $n_x = 25 - 1200$[20,21]. Since synthetic control of network topology is limited, we performed coarse-grained molecular dynamics simulations of linear chain and diamond networks that allow accurate variations of strand dimensions, effective crosslinking functionality, and defects distribution (Supplementary Information).

We first apply the forensic approach to results of molecular dynamics simulations of *phantom networks*[1,22] made by crosslinking of noninteracting bead-spring chains (precursor chains) with degree of polymerization (DP) $N = 1025$ in a melt state (Supporting Information). The networks have dangling ends and loops, but are without entanglements as network strands are permitted to cross each other. The equation of state for phantom networks undergoing uniaxial elongation, λ, under true stress, σ_{true}, is derived by considering individual network strands as nonlinear springs of finite extensibility[3,23]

$$\sigma_{true}(\lambda) = (\lambda^2 - \lambda^{-1})\frac{G}{3}\left[1 + 2\left(1 - \frac{\beta(\lambda^2 + 2\lambda^{-1})}{3}\right)^{-2}\right] \quad (1)$$

which results in appearance of the divergent term in the brackets. The strain-stiffening behavior is defined by the firmness parameter

$$\beta \equiv \langle R_{in}^2 \rangle / R_{max}^2 = \alpha\left(1 - \frac{\alpha}{2}\left(1 - exp\left(-\frac{2}{\alpha}\right)\right)\right) \quad (2)$$

Eq 2 characterizes the strand extensibility, i.e. how much a network strand with a degree of polymerization (DP) n_x between crosslinks and the repeat unit projection length l can be stretched from its initial mean-square end-to-end distance $\langle R_{in}^2 \rangle$ to the fully extended state R_{max}=$n_x l$. The second part of eq 2 expresses β in terms of $\alpha^{-1} = n_x l / b_K$ - the number of Kuhn segments of length b_K per network strand. The structural shear modulus of phantom networks, G, includes contributions from stress-supporting strands between crosslinks with functionality f, dangling ends, and loops as

$$G = \frac{G_m}{n_x} \frac{\langle R_{in}^2 \rangle}{b_K R_{max}} \left(1 - \frac{2}{\langle f \rangle}\right) C_{loop} \left(1 - \frac{n_x}{N}\right) \quad (3)$$

where $G_m = \rho k_B T$ is the monomeric shear modulus defined by the monomer number density ρ and the thermal energy $k_B T$. The coefficient C_{loop} describes the reduction of G due to loops (inset in Fig. 2a), while the factor $1 - n_x/N$ quantifies the decrease in the density of stress-supporting strands caused by two dangling ends per precursor chain and having $n_x/2$ monomers each (inset in Fig. 2a and Supporting Information).[1,2] In addition, the dangling ends reduce the effective crosslink functionality, which is accounted for by using the average value of the crosslink functionality $\langle f \rangle$ (Supplementary Equations 2-5).

Figure 2 outlines the main steps of the forensic approach in application to a set of phantom networks with different crosslink densities. First, structural shear modulus G and strand extensibility parameter β are determined for each network by fitting the corresponding stress-elongation curves with eq 1 (Fig. 2a). Second, we solve eq 2 for α and calculate the number of bonds in the network strands between crosslinks $n_{x,calc} = b_K / l\alpha$ by using the known ratio b_K/l=2.56, which appeared to be within 8% of the actual n_x values (Supplementary Figure 1d).

Third, the DP of the precursor chains, N, and loop coefficient, C_{loop}, are obtained by rearranging eq 3 as follows

$$G = G_m \frac{\beta}{\alpha}\left(1 - \frac{2}{\langle f \rangle}\right) C_{loop}\left(\frac{l}{b_K}\alpha - \frac{1}{N}\right) \quad (4)$$

and plotting normalized structural modulus $G\alpha/G_m\beta$ as a function of α (Fig. 2b). It is important to point out that the C_{loop} includes contributions from all types of loops as well as higher order corrections due to dangling-ends that are omitted in the analytical calculations of the loop factor.[10,24] Using the known b_K/l=2.56, the values of the slope and intercept give $(1 - 2/\langle f \rangle)C_{loop} \approx 0.40 \pm 0.01$ and degree of polymerization of the precursor chains N_{calc}=998, which is close to the actual value 1025. Since $\langle f \rangle$ depends on n_x/N ratio (Supplementary Equation 5), we can use obtained values of n_x and N to calculate $\langle f \rangle$ and represent the loop coefficient C_{loop} in terms of $\langle f \rangle$ (Fig. 2c).

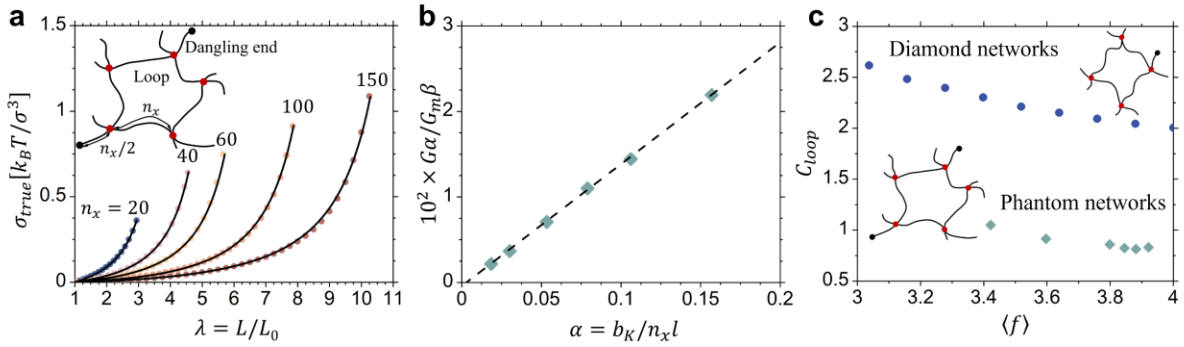

Figure 2. Forensics of phantom networks. a, Stress-elongation curves obtained by computer simulations of phantom networks with different crosslink densities made by crosslinking linear bead-spring chains with bead diameter σ and the degree of polymerization $N = 1025$ undergoing uniaxial deformation from initial size L_0 to L described by the elongation ratio $\lambda = L/L_0$. Solid lines are the best fits to eq 1 by considering G and β as fitting parameters (Supplementary Table 1). **b,** Self-similarity of phantom networks of linear chains is confirmed by plotting $\frac{G\alpha}{G_m\beta}$ as a function of parameter $\alpha = b_K/n_x l$, which effectively corresponds to strand DP n_x ($G_m = 0.85\ k_BT/\sigma^3$). The dashed line is the best fits to the equation $y = 0.143x - 0.00041$. **c**, Dependence of the loop coefficient C_{loop} on the average crosslink functionality $\langle f \rangle$ for linear chain networks (filled rhombs) and diamond networks of end-linked chains with $n_x = 150$ and different density of dangling ends (filled circles).

Similar analysis can be applied to *diamond networks* of end-crosslinked phantom strands with varying density of dangling ends (inset in Fig 2c, Supplementary Figure 1c and Table 1). A perfect diamond network without dangling chains has crosslink functionality $f = 4$ and can be viewed as a hierarchical system of loops with $C_{loop} = 2$ (Fig. 2c). Dangles lead to a decrease of average $\langle f \rangle$ and increase C_{loop}, which scales inversely with $\langle f \rangle$. Thus, the forensic approach executed on model networks provides complete information about the DP between crosslinks, effective crosslink functionality, as well as quantifies the effect of loops and dangling ends on the network elasticity.

The stress-strain analysis becomes more complex for real networks with trapped entanglements, described by the following non-linear equation of state[3,23]

$$\sigma_{true}(\lambda) = (\lambda^2 - \lambda^{-1})\left(\frac{G_e}{\lambda} + \frac{G}{3}\left[1 + 2\left(1 - \frac{\beta(\lambda^2 + 2\lambda^{-1})}{3}\right)^{-2}\right]\right) \quad (5)$$

where G_e represents the direct contribution of entanglements to stress support and corresponds to different mode of network deformation. In addition, entanglements cause an indirect effect on the structural modulus as

$$G = G_m \frac{\beta}{\alpha}\left(1 - \frac{2}{f}\right)\left(\frac{1}{n_x} + \frac{1}{n_{eff}}\right) \quad (6)$$

Where n_{eff} describes partitioning of repeat units between stress-supporting structural elements (networks strands, entanglement strands, and loops) and stress-free elements (dangling ends). The sign "+" indicates that entanglements enhance stiffness by overpowering the contributions from strands, dangles, and loops. Unlike model networks with specific incorporated defects[10] and ones discussed above, the partitioning representation is more adequate for real networks given the unfeasibility in separating individual contributions from specific elements of unknown network

topology. Furthermore, this approach has proven to be instrumental in elucidating the interplay of entanglements and chemical crosslinks as discussed below.

We apply eqs 5 and 6 to monitor the evolution of mechanical properties of natural rubber upon increasing crosslink density (Supplementary Figures 4-6) [19]. Two distinct deformation regimes with $G < G_e$ and $G > G_e$ separated by a sharp transition at $\beta \approx \alpha$=0.027 were identified (Fig. 3a). From the slope value a=0.13 at β>0.027 and the known b_K/l=1.89 and f=4, we estimate $\langle n_x \rangle = n_x^* = 0.5/a\beta \approx 143$, which corresponds to the transition at β=0.027 and accounts for strand polydispersity (Supplementary Equations 10-15). Since, n_x^* is larger than the entanglement DP in a melt of precursor chains $n_e \approx 57$ [25], we argue that there is a percolation-like transition[26] between two types of networks, where elasticity is controlled by either crosslinks ($\langle n_x \rangle < n_x^*$) or entanglements ($\langle n_x \rangle > n_x^*$) (insets in Fig. 4a). In these networks, the entanglement contributions (before and after n_x^*) are qualitatively different, which results in the stepwise G increase and change in its functional form. This is corroborated by the dependence of the shear modulus at small deformations (G_0) on the ratio $n_e/\langle n_x \rangle$ for natural rubber and tetrafunctional ($f = 4$) networks of end-crosslinked PDMS chains (Fig. 3b) [9]. Even though the networks differ in both chemistry and topology, they demonstrate the same percolation behavior during a crosslinking process: a sharp increase in shear modulus at $\langle n_x \rangle = n_x^*$ followed by a linear increase of modulus for $\langle n_x \rangle < n_x^*$. In the entanglement-controlled regime, $n_x^* < \langle n_x \rangle$, the plateau modulus of the PDMS networks is close to that of entangled linear PDMS melt (G_e=0.2 MPa). In contrast, the majority of the natural rubber samples are softer than G_e= 0.58 MPa [25], which suggests a dilution of entanglements during the network formation. This finding calls into question the commonly held belief of continuous crossover between two types of networks[8,22] and should be a subject of future research.

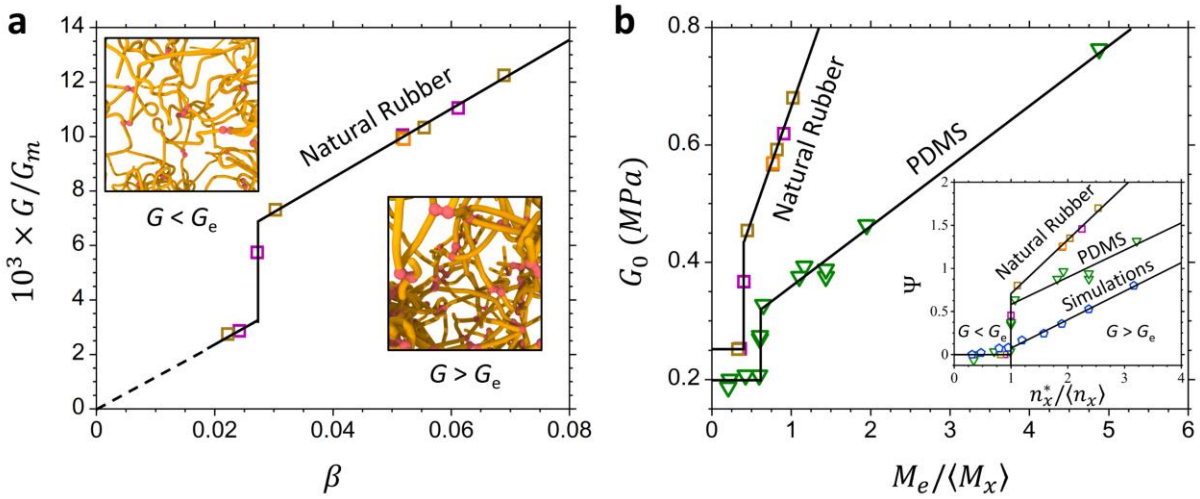

Figure 3. Elasticity and percolation transition. a, Evolution of the reduced structural shear modulus G/G_m with the firmness parameter β for natural rubber crosslinked in a melt of chains with M_n=195kg/mol at 25°C ($f = 4$ and $G_m = 33.16\,MPa$). The solid line corresponds to the equation: $G/G_m = 0.5\left(\frac{n_x(\alpha)}{\langle n_x\rangle}\frac{l}{b_K}\beta + \frac{1}{n_{eff}}\right) = 0.13\beta + 0.0033$, for β>0.027. The factor $n_x(\alpha)/\langle n_x\rangle \approx 2$ accounts for renormalization of the DP of network strands due to effects of strand polydispersity. The dashed-solid line in the interval β<0.027 indicates extrapolation to infinitely long strands with $\beta = 0$. The insets show computer simulation snapshots for entanglements-controlled ($G < G_e$) and crosslinks-controlled ($G > G_e$) networks. **b,** Shear modulus at small deformations $G_0 \equiv \frac{1}{3}(\partial\sigma/\partial\lambda)_{\lambda=1} = G_e + G(1 + 2(1-\beta)^{-2})/3$ as a function of the ratio $M_e/\langle M_x\rangle$ for randomly crosslinked natural rubber and tetrafunctional PDMS networks of end-crosslinked chains of different molecular weights. In PDMS networks, the number average strand mass $\langle M_x\rangle$ varies between 2460 and 58000 g/mol, while the entanglement molecular weight in a PDMS melt is M_e= 12000 *g/mol*. Solid lines show general trends. Inset shows normalized shear modulus $\Psi = (G_0 - G_{av})/G_{av}$ on the ratio $n_x^*/\langle n_x\rangle$ for different networks as indicated. Coarse-grained networks studied in computer simulations are made by crosslinking chains with DP=1025 in a melt (open pentagons). Shear modulus G_{av} corresponds to the average value in the plateau regime and n_x^* defines the location of the percolation transition. The sharpness of the transition is a general feature for all networks studied experimentally. However, in computer simulations, the sharp transition transforms into a crossover due to finite size effect.

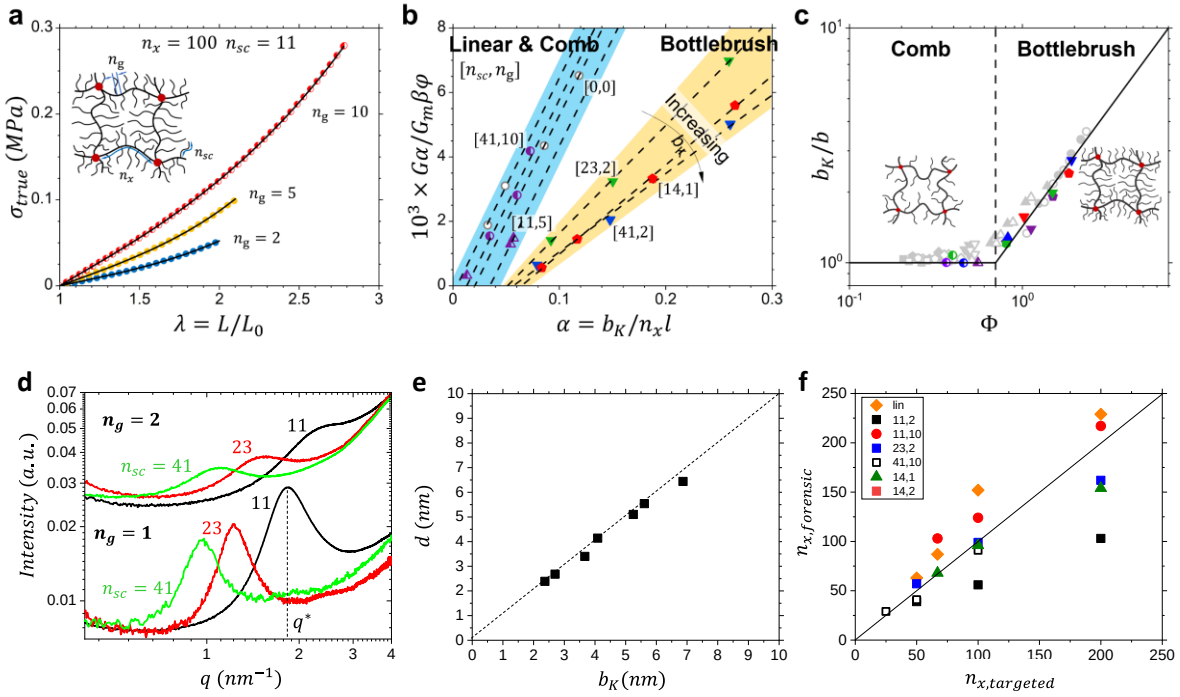

Figure 4. Forensics of brush network elasticity. a, Examples of stress-elongation curves measured upon uniaxial extension of PBA brush elastomer with different grafting densities as indicated. Solid lines are the best fits to eq 5 by considering G_e, G, and β as fitting parameters (Supplementary Table 4). **b,** The reduced structural shear modulus $\frac{G\alpha}{G_m\beta\varphi} = \left(1 - \frac{2}{f}\right)\left(\frac{l}{b_K}\alpha - \frac{1}{n_{eff}}\right)$ versus parameter α for linear, comb, and bottlebrush PBA networks ($f = 4$ and $G_m = 20.83$ MPa). The sign "−" in front of $1/n_{eff}$ term indicates weak effect of entanglements on elasticity for this type of networks. The dashed lines are the best fits to the equation $y = ax - c$, where the slope a and intercept c give b_K and n_{eff}, respectively. The fits give the following (a, c) coefficients for the corresponding $[n_g, n_{sc}]$ pairs for networks with PBA linear [(0.067,0.0014),[0,0];(0.067,0.0002),[0,0]], PBA comb [(0.067,0.0023), [11,5]; (0.066,0.0009) ,[11,10]], PBA bottlebrush [(0.033,0.0017),[23,2]; (0.024,0.0014),[41,2]], and PDMS bottlebrush [(0.028,0.0018), [14,1]] strands. **c,** The reduced Kuhn length, b_K/b, as a function of the crowding parameter, $\Phi = \varphi^{-1}{n_{sc}}^{-1/2}/\rho(bl)^{3/2}$ for PBA and PDMS brush polymers as well as computer simulations data (grey symbols) [22,26]. The vertical dashed line shows the crossover between the comb and bottlebrush regimes at $\Phi = \Phi^* \cong 0.7$ [28,29]. The legend for symbols is given in Supplementary Table 4. **d**, Small-angle X-ray scattering (SAXS) curves of PBA brush networks at fixed targeted n_x=100 (a) with n_g=1 and various DPs of side chains, n_{sc}. **e,** Correlation between bottlebrush diameter $d = 2\pi/q^*$ calculated from the peak position q^* in d and Kuhn length b_K obtained from forensic analysis. **f,** Correlation between the targeted degree of polymerization crosslinks and one calculated by using forensic approach.

Finally, we illustrate the applicability of the forensic approach to networks with brush-like strands, where stress-supporting backbones are diluted by side chains with DP=n_{sc} separated by n_{g} backbone repeat units defined by $\varphi = n_{\mathrm{g}}/(n_{\mathrm{g}} + n_{sc})$ (inset, Fig. 4a). Like for the linear chain networks with $n_{sc} = 0$ ($\varphi = 1$) (Fig.2a), the forensics procedure begins with fitting experimental stress-elongation curves (Fig. 4a) with eq 5 to obtain G and β values (Supplementary Tables 4-6). The Kuhn length b_K of brush backbone is determined from the slope of reduced structural shear modulus $G\alpha/G_m\beta\varphi$ as a function of α (Fig. 4b). For systems with lower grafting density (linear and comb-like networks), several parallel lines are observed with slopes equal to $(1 - 2/f)l/b_K$, which is consistent with the fact that b_K is not affected by loosely grafted side chains. The vertical shift between the lines reflects changes in the fraction of repeat units belonging to stress-supporting strands characterized by n_{eff}, including the contribution from trapped entanglements. Considering the known crosslink functionality f=4, the Kuhn length of linear and comb-like PBA chains are calculated as $b_K = b = 1.91$ nm, which is in excellent agreement with literature values b=1.79 −1.90 nm of the bare PBA backbone.

In densely grafted bottlebrush networks, the inverse relationship observed between slope and grafting density ($\varphi^{-1} = 1 + n_{sc}/n_{\mathrm{g}}$) is due to steric repulsion between side chains, resulting in backbone extension and stiffening. (Fig. 4b). To demonstrate the effect of side chains on strand stiffness, we plot the normalized Kuhn length b_K/b as a function of the so-called crowding parameter Φ, which describes the degree of interpenetration of side chains belonging to different brush molecules (Fig. 4c)[27,28]. In the comb regime ($\Phi < \Phi^*$), the steric repulsion between side chains is weak and the effective Kuhn length of the backbone is $b_K \approx b$[27,28]. However, in bottlebrush systems ($\Phi > \Phi^*$), the repulsion between densely grafted side chains results in

backbone stiffening as $b_K \approx b\Phi/\Phi^*$ [28,29]. The behavior is universal as it was observed for brush elastomers with chemically different side chains (PBA, PDMS)[20,21] as well as in molecular dynamics simulations of bottlebrush melts (Fig. 4c) [28,29]. The obtained b_K values were compared with the distance between brush backbone from small angle X-ray scattering. The intrinsic electron density contrast for the bottlebrush backbones with densely grafted side chains results in a distinct scattering peak corresponding to the brush diameter, $d = 2\pi/q^*$ (Fig. 4d).[21,21a] The excellent agreement between the bottlebrush diameter d and the Kuhn length obtained from forensic approach (Fig 4e) is consistent with analytical calculations and computer simulations of b_K in bottlebrush melts.[27,30]

Following the forensic protocol outlined above, we use the Kuhn length b_K and value of parameter α to calculate the DP between crosslinks, $n_{x,calc} = b_K/l\alpha$ (Supporting Table 4). The determined $n_{x,calc}$ scales linearly with targeted n_x, which corroborates self-similarity of the synthesized networks (Fig. 4f). The deviation in absolute numbers between the targeted and true n_x's is ascribed to inevitable variations of synthetic conditions between individual series which in turn influences the crosslinking efficiency.

Varying network topologies results in different patterns of stress distribution between structural elements. To quantify a network's effectiveness in absorbing an applied force, we introduce a quality factor, κ, defined as the ratio of the real network modulus G to that of the defect-free affine network model, G_{affine}, in which stress is evenly divided between all network strands[1,22]

$$\kappa = \frac{G}{G_{affine}} = \frac{G b_K}{G_m \beta l} \tag{7}$$

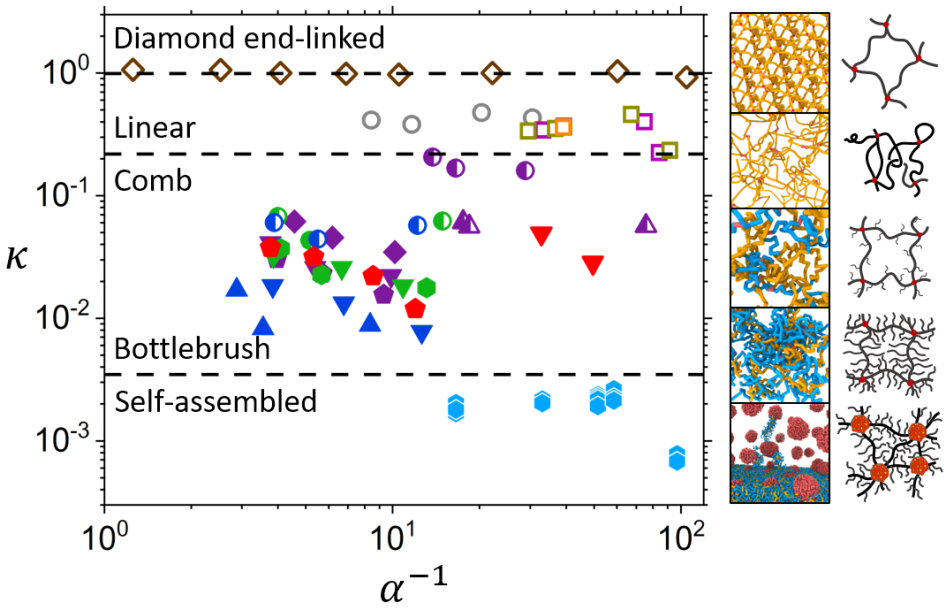

Figure 5. Network topology classification. a, Mapping of polymer networks with different topologies in terms of quality factor κ and number of Kuhn segments per network strand, $\alpha^{-1} = \tilde{n}_x l/b_K$. The analyzed networks include: end-crosslinked diamond networks studied in computer simulations (open rhombs), natural rubber (open squares), networks of comb (half-filled symbols) and bottlebrush (filled symbols) strands, and self-assembled network of linear-bottlebrush-linear (PMMA-PDMS-PMMA) copolymers (filled blue hexagons), (PMMA - poly(methyl methacrylate)). Legends for other symbols are given in Supplementary Tables 4-6. The pictures on the right show computer simulation snapshots of 3D network structure and schematics of network mesh.

This parameter is directly related to the topology of the stress-supporting scaffold (eq.3 and 6) and reduces to $\kappa = Gn_x/G_m$ for networks of linear flexible chains. Fig. 5 presents the quality factor for linear, brush-like, covalent, and self-assembled networks as a function of the number of Kuhn segments per network strands between crosslinks, $\alpha^{-1} \equiv n_x l/b_K$. For defect-free diamond networks, prepared by end-crosslinking of identical chains[31], κ = 1 indicating a uniform stress distribution independent on the DP between crosslinks. In real networks such as natural rubber[19], the uneven stress partitioning results in $\kappa < 1$ along with a downward trend change at $\alpha^{-1} \cong 70$, where a transition to the entanglement-controlled network elasticity occurs. Further reduction of κ is observed for networks with comb-like strands[20] due to a considerable fraction of stress-free

side chains and dangling ends. In bottlebrush networks[20], the increase of grafting density leads to an additional decrease of κ between 0.01 and 0.1 due to stiffening of the brush strands by steric repulsion between densely grafted side chains. For self-assembled networks of linear-bottlebrush-linear copolymers[21], the quality factor falls below the covalent brush networks (Supplementary Table 6). The worsening of the stress distribution in such networks is a result of stronger stretching of stress-supporting bottlebrush strands and their significant dilution by bulky network nodes formed upon self-assembly of the linear end blocks.

To summarize, we presented a forensic methodology for decoding the degree of polymerization of the stress-supporting strands, strand flexibility (Kuhn length), and network topology by analyzing the non-linear response of elastomers to deformation. The introduction of the quality factor, κ, established a universal classification of self-assembled and chemical networks made of strands with different molecular architectures according to the stress distribution between network structural elements. For natural rubber and PDMS networks, we discovered a percolation transition between networks with crosslink- and entanglement-controlled elasticity. Applying this technique to networks with brush-like strands elucidated the Kuhn length dependence on the brush molecular architecture. We believe that our approach will be a valuable technique for the characterization of synthetic and biological networks due to its simplicity and yet comprehensive explanatory power[7] for accurate prediction of their structures[3-6]. Furthermore, decoding the structure of real networks is crucial for the verification of architectural codes generated by future AI machinery in soft matter design. By comparing the AI-recommended and as-synthesized architectural codes, one will be able to optimize the synthesis conditions to achieve optimal mechanical properties.

Acknowledgments

This work was supported by the National Science Foundation under the grants DMR 1921835, DMR 1921923, DMR 2049518, and DMR 2004048. E.A.N. and D.A.I. acknowledge the Ministry of Science and Higher Education of the Russian Federation for financial support in the frame of state contract No 075-15-2022-1117 from June 30, 2022. A.V.D. and S.S.S. are grateful to Prof. Edward Samulski for the critical reading of the manuscript and numerous stimulating discussions. The authors acknowledge the contribution of Dr. Benjamin J. Morgan and Dr. Andrew N. Keith to the synthesis of well-defined PBA elastomers and linear-bottlebrush-linear copolymers reported previously. The authors acknowledge the European Synchrotron Radiation Facility (ESRF) for provision of synchrotron beamtime at the ID02 beamline and would like to thank the staff of the ESRF and Egor A. Bersenev for assistance.

Author Contributions

A.V.D. developed the concept and theoretical foundation; Y.T., F.V. and M.M. analyzed correlations between network structure and mechanical properties; M.J. and Y.T. performed molecular dynamics simulations of polymer networks and analyzed their properties; E.A.N. and D.A.I. performed X-ray scattering measurements and analyzed the structure of the bottlebrush copolymers, A.V.D. and S.S.S. were the primary writers of the manuscript and the principal investigators. All authors discussed the results and provided feedback on the manuscript.

Supplementary Information

Data analysis, computer simulation details.

REFERENCES

1 Treloar, L. R. G. *The Physics of Rubber Elasticity*. (Clarendon Press, 1975).
2 Flory, P. J. *Principles of Polymer Chemistry*. (Cornell University Press, 1971).
3 Sheiko, S. S. & Dobrynin, A. V. Architectural code for rubber elasticity: From supersoft to superfirm materials. *Macromolecules* **52**, 7531-7546 (2019).
4 McKenna, G. B. Soft matter: rubber and networks. *Rep. Prog. Phys.* **81**, 0666602 (2018).
5 Zhang, Y. S. & Khademhosseini, A. Advances in engineering hydrogels. *Science* **356** eaaf3627 (2017).
6 Peppas, N. A., Hilt, J. Z., Khademhosseini, A. & Langer, R. Hydrogels in biology and medicine: from molecular principles to bionanotechnology *Adv. Mater.* **18**, 1345–1360 (2006).
7 Danielsen, S. P. O. *et al.* Molecular characterization of polymer networks. *Chem. Rev.* **121**, 5042-5092 (2021).
8 Dossin, L. M. & Graessley, W. W. Rubber elasticity and well-characterized polybutadiene networks. *Macromolecules* **12**, 123-130 (1979).
9 Patel, S. K., Malone, S., Cohen, C., Gillmor, J. R. & Colby, R. H. Elastic-modulus and equilibrium swelling of poly(dimethylsiloxane) networks. *Macromolecules* **25**, 5241-5251 (1992).
10 Zhong, M., Wang, R., Kawamoto, K., Olsen, B. D. & Johnson, J. A. Quantifying the impact of molecular defects on polymer network elasticity. *Science* **353**, 1264-1268 (2016).
11 Smith, S. B., Cui, Y. J. & Bustamante, C. Overstretching B-DNA: The elastic response of individual double-stranded and single-stranded DNA molecules. *Science* **271**, 795-799 (1996).
12 Neuman, K. C., Lionnet, T. & Allemand, J. F. Single-molecule micromanipulation techniques. *Ann. Rev. Mater. Res.* **37**, 33-67 (2007).
13 Flory, P. J. Network topology and the theory of rubber elasticity. *Br. Polym. J.* **17**, 96-102 (1985).
14 Langley, N. R. Elasticity effective strand density in polymer networks. *Macromolecules* **1**, 348-352 (1968).
15 Miller, D. R. & Macosko, C. W. New derivation of post gel properties of network polymers. *Macromolecules* **9**, 206-211. (1976).
16 Sandakov, G. I., Smirnov, L. P., Sosikov, A. I., Summanen, K. T. & Volkova, N. N. NMR analysis of distribution of chain lengths between crosslinks of polymer networks. *J. Polym. Sci. Polym. Phys.* **32**, 1585–1592 (1994).
17 Bastide, J. & Candau, S. J. in *Physical Properties of Polymeric Gels* (ed J. P. Cohen) 143−308 (Wiley, 1996).
18 Edwards, S. F. & Vilgis, T. A. The tube model theory of rubber elasticity. *Rep. Prog. Phys.* **51**, 243-297 (1988).
19 Mullins, L. Determination of degree of crosslinking in natural rubber vulcanizates. Part IV. Stress-strain behavior at large extensions. *J. Appl. Polym. Sci.* **2**, 257-263 (1959).
20 Vatankhah-Varnosfaderani, M. *et al.* Mimicking biological stress-strain behaviour with synthetic elastomers. *Nature* **549**, 497-501 (2017).
21 Vatankhah-Varnosfaderani, M. *et al.* Chameleon-like elastomers with molecularly encoded strain-adaptive stiffening and coloration. *Science* **359**, 1509-1513 (2018).
21a Maw, M., et al. *Macromolecules* **55**, 2940−2951 (2022).
22 Rubinstein, M. & Colby, R. H. *Polymer Physics*. (Oxford University Press, 2003).
23 Dobrynin, A. V. & Carrillo, J.-M. Y. Universality in nonlinear elasticity of biological and polymeric networks and gels. *Macromolecules* **44**, 140-146 (2011).
24 Panyukov, S. Loops in polymer networks. *Macromolecules* **52**, 4145−4153 (2019).
25 Fetters, L. J., Lohse, D. J. & Colby, R. H. in *Physical Properties of Polymers Handbook* (ed J. E. Mark) 445-452 (Springer, 2007).
26 Staufer, D. *Introduction to Percolation Theory*. (Taylor and Francis, 1985).

27 Daniel, W. F. M. *et al.* Solvent-free, supersoft and superelastic bottlebrush melts and networks. *Nature Materials* **15**, 183-189 (2016).
28 Liang, H., Cao, Z., Wang, Z., Sheiko, S. S. & Dobrynin, A. V. Combs and bottlebrushes in a melt. *Macromolecules* **50**, 3430-3437 (2017).
29 Liang, H., Wang, Z., Sheiko, S. S. & Dobrynin, A. V. Comb and bottlebrush graft copolymers in a melt. *Macromolecules* **52**, 3942−3950 (2019).
30 Cao, Z., Carrillo, J.-M. Y., Sheiko, S. S. & Dobrynin, A. V. Computer simulations of bottle brushes: from melts to soft networks. *Macromolecules* **48**, 5006-5015, doi:10.1021/acs.macromol.5b00682 (2015).
31 Carrillo, J.-M. Y., MacKintosh, F. C. & Dobrynin, A. V. Nonlinear elasticity: from single chain to networks and gels. *Macromolecules* **46**, 3679-3692 (2013).